# Large eddy simulation of boundary layer transition flow around NACA0009 blunt trailing edge hydrofoil at high Reynolds number

**J Chen**[1], **Y J Li**[1, 2,*] **and Z Q Liu**[1, 2]
[1] College of Water Resources and Civil Engineering, China Agricultural University, Beijing 100083, China
[2] Beijing Engineering Research Center of Safety and Energy Saving Technology for Water Supply Network System, Beijing 100083, China

[*]Corresponding author, E-mail address: liyaojun@cau.edu.cn

**Abstract:** The process of boundary layer transition is needed to be taken into account for better understanding of the flow around a hydrofoil. Based on the WALE model, this paper presents a large eddy simulation of the flow around NACA0009 blunt trailing edge hydrofoil to investigate the characteristics of the boundary layer transition at high Reynolds number. The accuracy of the WALE model in predicting the transition process is validated by comparing the calculated boundary layer velocity profiles, thicknesses and shape factors with experimental data. Moreover, the spatial development laws of velocity fluctuation in the transitional boundary layer are revealed by analyzing the profiles of resolved normal and shear Reynolds stress in both streamwise and transverse directions

## 1. Introduction

Boundary layer transition is a typical phenomenon in the flow around hydrofoil and have a great influence on the hydrodynamic characteristics such as lift, drag and vortex shedding. Therefore, boundary layer transition is needed to be predicted accurately for better understanding of the flow around a hydrofoil. DNS (Direct Numerical Simulation) is the best way to simulate transition, but this process requires a prohibitive amount of computational resources. To save computing resources, three main methods, namely the $e^N$ method[1] [2], the laminar kinetic model[3][4] and the intermittency model[5] are used widely for the transition prediction in engineering applications at present. The $e^N$ method is based on linear stability theory and estimates transition using the growth ratio of downstream fluctuation to original fluctuation. This method is difficult to use due to the main challenge of estimating the factor $N$, which can be varied for different flows[6]. Both the laminar kinetic model and the intermittency model are based on conventional RANS turbulence model, like the SST $k-\omega$ model, so the computational expense is comparatively low. But the precision of these two methods in transition prediction is heavily depended on empirical function, which makes them have significant limitations in conditions where the flow parameters are beyond the calibration range of the empirical function.

In the past decades, large eddy simulation (LES) has been used widely and validated extensively in the simulation of turbulent flow. In LES, the large-scale eddies of flow, which carry the majority of the energy are resolved directly, and the small-scale eddies are modeled via a subgrid-scale stress (SGS)

model. Different SGS models have been proposed to model the kinetic energy contained by the filtered turbulence. For a transitional flow, the kinetic energy is zero in laminar region and will grow gradually in transition region, so the construction of SGS model is crucial to simulate transition accurately. The conventional SGS model, like the Smagorinsky model[7], is believed to be unable to reproduce transition process because the subgrid-scale eddy viscosity calculated by the model is too large in laminar region[8]. The Wall-Adapting local Eddy Viscosity (WALE) model[8], which based on the square of the velocity gradient tensor so that the eddy viscosity is almost zero in wall-bounded laminar flow, have the ability in theory to simulate laminar flow and the development of linearly unstable wave. Therefore, the WALE model-based large eddy simulation has been applied to the investigation of boundary layer transition in recent years[9][10][11]. But given that these applications are mainly under low or middle Reynolds number, the accuracy of the WALE model in predicting the transition over curvature surface at high Reynolds number is needed to be further validated. Moreover, sometimes we are more interested in the development laws of turbulent fluctuation in boundary layer transition, which is helpful for the study on transition mechanism, as well as the setup and calibration of empirical transition model. But these kinds of studies are quite insufficient.

So in this paper, we present a large eddy simulation of the boundary layer transition flow around the NACA0009 blunt trailing edge hydrofoil based on the WALE model. The capability of the WALE model in predicting the transition process is validated by analyzing the boundary layer structures of the calculation and the experiment. Besides, streamwise and transverse velocity fluctuations are analyzed to reveal the spatial development laws in the transitional boundary layer flow over the hydrofoil at high Reynolds number.

## 2. Numerical model and methods

### *2.1. WALE model*

The WALE model[8] is used in the large eddy simulation for the closure of the unknown subgrid-scale stress, $\tau_{ij}$, induced by the filtering operation of subgrid-scale eddies. The expression of $\tau_{ij}$ in WALE model is given by

$$\tau_{ij} = -2\rho\nu_t\bar{S}_{ij} + \frac{1}{3}\tau_{kk}\delta_{ij} \tag{1}$$

where $\bar{S}_{ij}$ presents the filtered strain rate tensors, $\bar{S}_{ij} = 0.5\left(\partial\bar{u}_i/\partial x_j + \partial\bar{u}_j/\partial x_i\right)$. $\nu_t$ is the subgrid-scale turbulent eddy viscosity, and is defined as

$$\nu_t = \left(C_w\Delta\right)^2 \frac{\left(S_{ij}^d S_{ij}^d\right)^{3/2}}{\left(\bar{S}_{ij}\bar{S}_{ij}\right)^{5/2} + \left(S_{ij}^d S_{ij}^d\right)^{5/4}} \tag{2}$$

where $C_w$ is a constant and $\Delta$ is the filtered scale. $\bar{S}_{ij}$ denotes the traceless symmetric part of the square of the velocity gradient tensor, and it reads:

$$S_{ij}^d = \bar{S}_{ik}\bar{S}_{kj} + \bar{\Omega}_{ik}\bar{\Omega}_{kj} - \frac{1}{3}\left(\bar{S}_{mn}\bar{S}_{mn} - \bar{\Omega}_{mn}\bar{\Omega}_{mn}\right) \tag{3}$$

$$S_{ij}^d S_{ij}^d = \frac{1}{6}\left(\left(\bar{S}_{ij}\bar{S}_{ij}\right)^2 + \left(\bar{\Omega}_{ij}\bar{\Omega}_{ij}\right)^2\right) + \frac{2}{3}\bar{S}_{ij}\bar{S}_{ij}\bar{\Omega}_{lj}\bar{\Omega}_{lj} + 2\bar{S}_{ik}\bar{S}_{kj}\bar{\Omega}_{jl}\bar{\Omega}_{li} \tag{4}$$

where the filtered rotation rate tensors $\bar{\Omega}_{ij} = 0.5\left(\partial\bar{u}_i/\partial x_j - \partial\bar{u}_j/\partial x_i\right)$. From the construction of the equation (4), the WALE model based on $S_{ij}^d S_{ij}^d$ can reflect the effect of both the strain rate and the rotation rate of turbulence, which makes it have a significant difference to the conventional linear SGS model. In addition, except for the velocity gradient in wall-normal direction, $\partial\bar{u}_1/\partial x_2$, all the $\partial\bar{u}_i/\partial x_j$ terms are equal to zero in the pure shear flow. This means that $\bar{S}_{12}, \bar{S}_{21}, \bar{\Omega}_{12}, \bar{\Omega}_{21}$ are the only four nonzero terms, and $\bar{S}_{12} = \bar{S}_{21} = \bar{\Omega}_{12} = -\bar{\Omega}_{21}$. In the pure shear layer equation (4) yields

$$S_{ij}^d S_{ij}^d = \left[ \bar{S}_{ik}\bar{S}_{kj} + \bar{\Omega}_{ik}\bar{\Omega}_{kj} - \frac{1}{3}\delta_{ij}\left(\bar{S}_{mn}\bar{S}_{mn} - \bar{\Omega}_{mn}\bar{\Omega}_{mn}\right)\right]\left[ \bar{S}_{ik}\bar{S}_{kj} + \bar{\Omega}_{ik}\bar{\Omega}_{kj} - \frac{1}{3}\delta_{ij}\left(\bar{S}_{mn}\bar{S}_{mn} - \bar{\Omega}_{mn}\bar{\Omega}_{mn}\right)\right]$$
$$= \left[ \bar{S}_{12}\bar{S}_{21} + \bar{\Omega}_{12}\bar{\Omega}_{21} - \frac{1}{3}\left(\bar{S}_{12}\bar{S}_{12} + \bar{S}_{21}\bar{S}_{21} - \bar{\Omega}_{12}\bar{\Omega}_{12} - \bar{\Omega}_{21}\bar{\Omega}_{21}\right)\right]^2 + \quad (5)$$
$$\left[ \bar{S}_{21}\bar{S}_{12} + \bar{\Omega}_{21}\bar{\Omega}_{12} - \frac{1}{3}\left(\bar{S}_{12}\bar{S}_{12} + \bar{S}_{21}\bar{S}_{21} - \bar{\Omega}_{12}\bar{\Omega}_{12} - \bar{\Omega}_{21}\bar{\Omega}_{21}\right)\right]^2 = 0$$

In this case $\nu_t$ in equation (2) is equal to zero, so no modeled turbulence is produced by the WALE model in the pure shear flow (laminar) region. Actually DNS is implemented to the flow in this region, in that the development of linear unstable waves can be simulated. This is the key and theory for the WALE model to predict the laminar boundary layer and boundary layer transition.

*2.2. Solution strategy*

The filtered transient N-S equation is discretized by the finite volume method and the implicit time integration scheme. The second-order central-difference scheme is used for the advection term and the diffusion term. The second-order backward Euler scheme is used for the transient term. The coupled solution method is used to solve the discretized equations, and the algebraic multigrid method is used for the acceleration of calculation convergence. The dimensionless time step is set to $\Delta t^* = U\Delta t/L = 0.001$ (the average courant number is equal to 0.4), where $\Delta t$ is the physical time step and $U$ is the mean velocity at the inlet. The transient statistics are started after the solution goes into a steady state, and the dimensionless statistical time $t^* = Ut/L = 22$ (corresponding to a physical time of 2 flow-through), where $t$ is the physical time for flow statistics.

*2.3. Mesh and boundary condition*

Figure 1 shows the details of NACA0009 blunt trailing edge hydrofoil and the computational domain with $11L \times 1.5L \times 0.2L$ ($L$=100mm, where $L$ is the chord length of the hydrofoil). The inlet of the computational domain is extended to 4$L$ upstream of the leading edge of the hydrofoil to make the flow fully developed. To reduce computational expense, the spanwise size, $b$, is set to 0.2$L$ and periodic boundary condition is implemented as shown in Figure 1.

Hexahedral mesh is applied to discretize the computational domain. The total nodes of the mesh is about 5.0 million, and the average $y^+$ on the whole hydrofoil surface is about 0.6, which is sufficient to fully solve the near-wall flow. Correspondingly, the three walls in Fig.1 are set to be no-slip wall with no implementation of wall function. Uniform velocity ($U = 20\,\mathrm{m/s}$, $Re_L = 2\times10^6$) and static pressure are conducted at the inlet and outlet respectively.

Figure 2 shows the Power Spectrum Density (PSD) of velocity fluctuation in the full turbulent boundary layer. One can clearly see the $f^{-5/3}$ law, which means that the resolved turbulent scale is located in the inertial subrange. This also indicates that the mesh used in this simulation is sufficient. To investigate the reasonability of the spanwise size of the computational domain, Figure 3 presents the profiles of the spatial two point velocity correlation along hydrofoil spanwise direction. It is show that the correlation value can descend to near zero with the increase of distance to the wall, which indicates that the calculated results are independent of the spanwise size in this simulation.

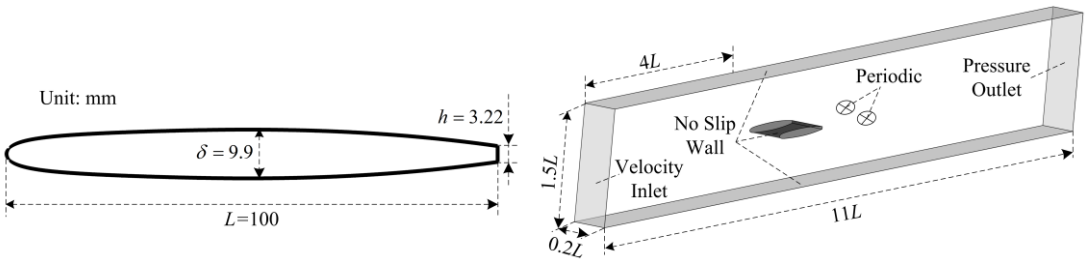


**Figure 1.** The details of the NACA0009 blunt trailing edge hydrofoil, computational domain and boundary conditions

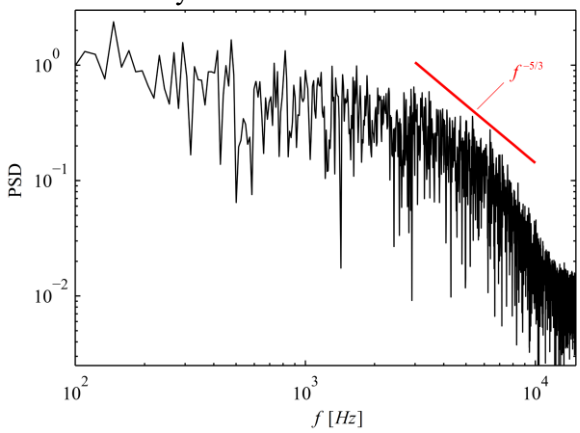


**Figure 2.** The power spectrum density of velocity fluctuation in the full turbulent boundary layer

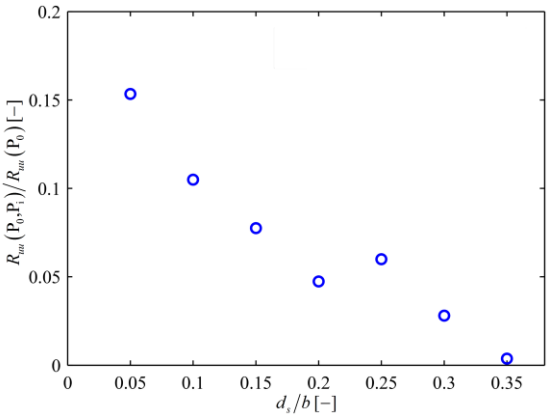


**Figure 3.** The profiles of spatial two point velocity correlation in the spanwise direction

## 3. Results

The aim of the simulation in this paper is to validate the capability of the WALE model in predicting the hydrofoil boundary layer transition at high Reynolds number, and to reveal the spatial development laws of velocity fluctuation during the transition.

### *3.1. Transitional boundary layer structure*

The time-averaged velocity profiles along hydrofoil chord are shown in Figure 4, including the data measured by the experiment[12] and the results calculated by the WALE model. In the figure, $d_w$ is the normal distance to the wall, and $U_t$ is the surface-tangent velocity, which is normalized by the external velocity, $U_{te}$. The good agreement between experiment and calculation means that the WALE model achieves better simulation for the transitional boundary layer. Figure 5 shows the boundary layer thickness profiles along hydrofoil chord. One can clearly see that the thickness increases slowly before $0.7L$ (streamwise location), but grows rapidly in the downstream of $0.7L$.

The boundary layer shape factor profiles along hydrofoil chord are shown in Figure 6 to better present the state of the boundary layer at different streamwise locations. The shape factor, $H_{12}$, is calculated by the boundary layer displacement thickness and boundary layer momentum thickness. Generally speaking, boundary layer is laminar state as $H_{12}$ larger than 2.6, while is turbulent state as $H_{12}$ smaller than 1.5. Between 1.5 and 2.6, the boundary layer is transitional state[12]. Both simulation results and experimental data show that the $H_{12}$ decreases rapidly in the downstream of $0.7L$. In this process, the boundary layer transfers to full turbulent state qucikly, making the boundary layer thickness increases rapidly, as shown in Figure 5.

Figure 7 shows the instantaneous eddy structures in the boundary layer and the wake region of the

hydrofoil. The surface eddies first start to appear in a small region near 0.6*L*, and then occupy the whole spanwise direction at 0.7*L*. But these eddies between 0.6*L* and 0.7*L* seem to be isolated, and the interaction among eddies is weak. In the downstream of 0.7*L*, more eddies appear and the spanwise interaction is becoming stronger, which brings the combination of eddies, leads to a much more complex and larger 3D eddies and speeds up the boundary layer transition process. In addition, the wake eddies also have strong interaction and show obvious 3D structure in the spanwise direction due to the higher Reynolds number. But one can still observe the regular array of discrete eddies that formed by the two shear layers from the detachment of the boundary layer on both upper and lower surfaces. These eddies shed from the trailing edge periodically, which can lead to the fluctuation of lift and drag.

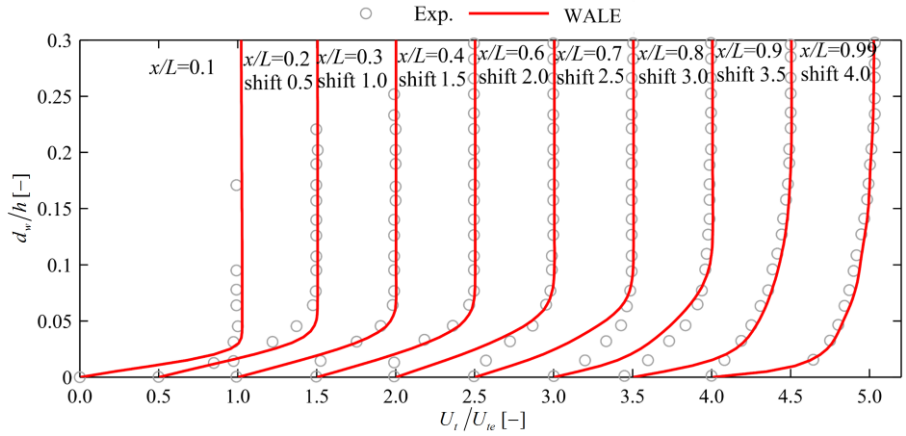


**Figure 4.** Boundary layer tangential time-averaged velocity profiles along hydrofoil chord

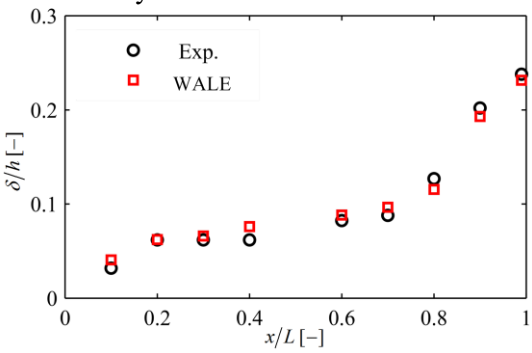


**Figure 5.** Boundary layer thickness profiles along hydrofoil chord

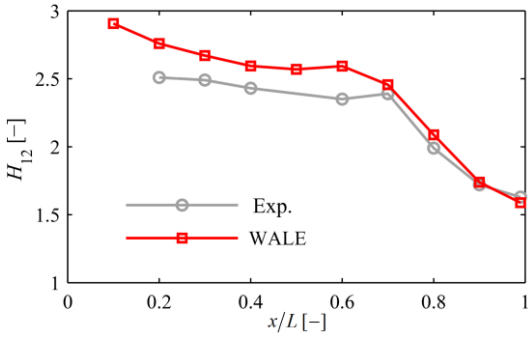


**Figure 6.** Boundary layer shape factor profiles along hydrofoil chord

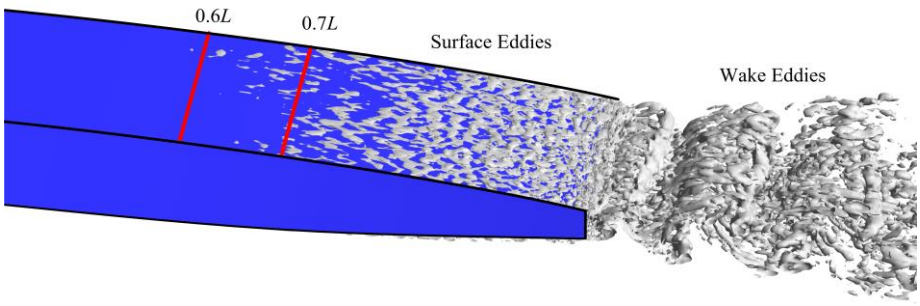


**Figure 7.** Instantaneous eddy structures (showed by the isosurface of $Q$, $Q = 2\times10^{7}\ [\mathrm{s}^{-2}]$)

*3.2. Development of velocity fluctuation*

Boundary layer transition is actually a process of fluctuation development, so it is important to investigate the development laws of the fluctuation during transition. Figure 8 shows the profiles of the double correlation of velocity fluctuation, (a) $\overline{u'u'}$, (b) $\overline{v'v'}$ and (c) $\overline{u'v'}$ along three isolines of mean velocity in the boundary layer, which actually represent three different layers of the boundary layer. In Figure 8(a) and Figure 8(b), it is clear that the fluctuation keeps a low value before 0.6$L$, but increases dramatically behind this location. Finally the fluctuation achieves the maximum value after 0.8$L$. It is show that the peak locations are almost same for the three isolines. The developments of $\overline{u'v'}$ in Figure 8(c) have the same trend as in Figure 8(a) and in Figure 8(b), apart from the profiles in the upper boundary layer. The value of $\overline{u'v'}$ in the upper boundary layer is opposite to the lower boundary layer because of the geometrical symmetry of the hydrofoil.

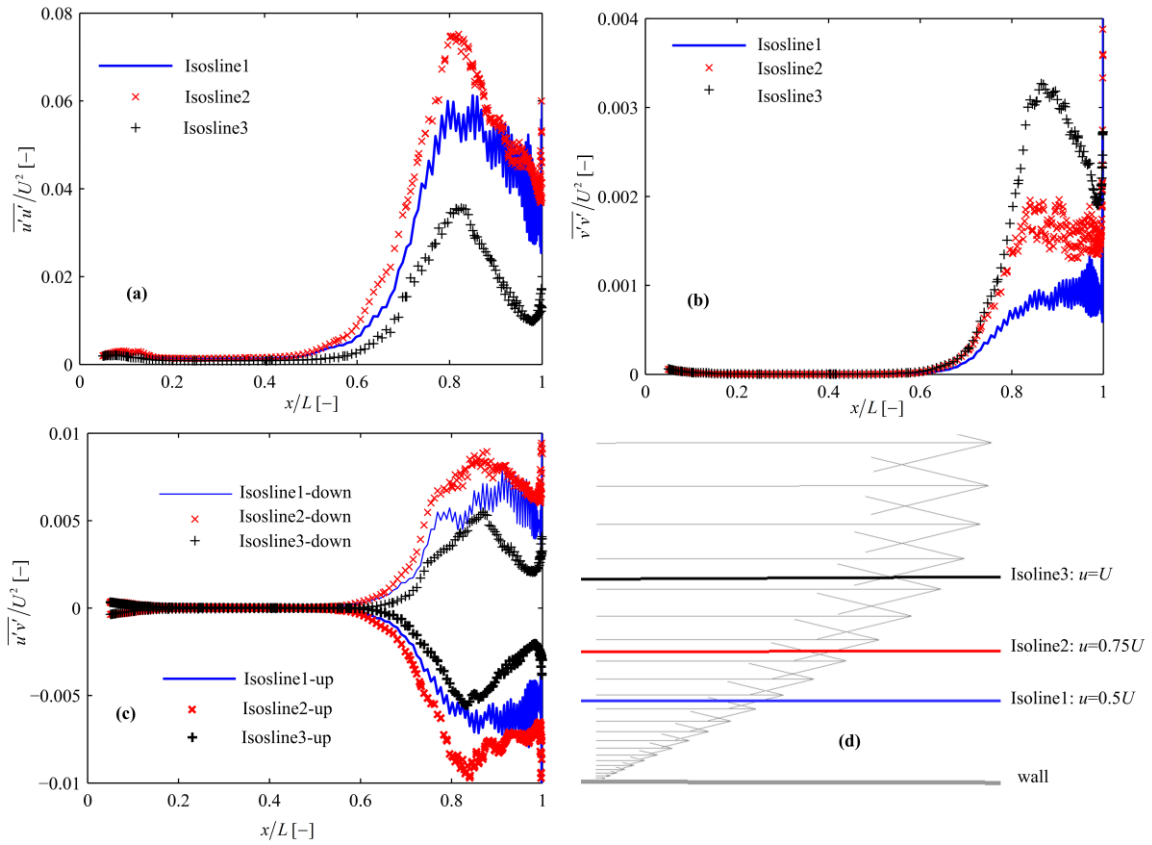


**Figure 8.** The profiles of double correlation of velocity fluctuation, (a) $\overline{u'u'}$, (b) $\overline{v'v'}$ and (c) $\overline{u'v'}$ along (d) the isoline of mean velocity in the boundary layer

Figure 9 shows the profiles of the growth ratio of velocity fluctuation along the three lines, where the growth ratio is calculated by dividing the local fluctuation by the fluctuation at 0.3$L$ (can be regarded as the laminar fluctuation). A phenomenon can be seen from the figure is that, although the profiles of the fluctuation for the three isolines are significantly different as shown in Figure 8, the profiles of the growth ratio are almost equal before achieving the peak value where the transition is accomplished. This means that the process of boundary layer transition is similar for the three isolines. Behind the peak location, the profiles of the ratio are obviously different because of the appearance of full turbulent boundary layer.

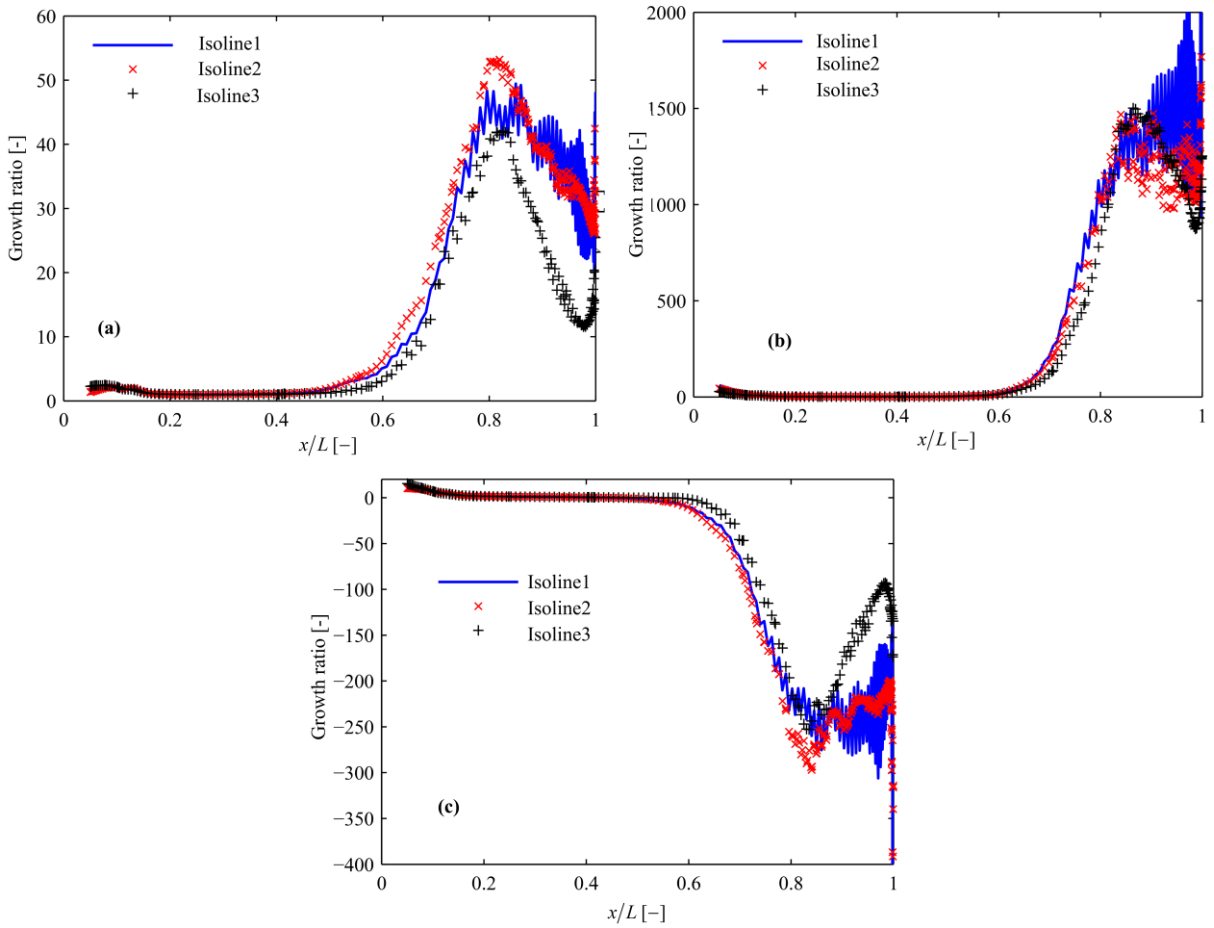


**Figure 9.** The profiles of the ratio of local fluctuation to the fluctuation at $0.3L$ along the isoline of mean velocity in the boundary layer: (a) $\overline{u'u'}/(\overline{u'u'})_{0.3L}$, (b) $\overline{v'v'}/(\overline{v'v'})_{0.3L}$, (c) $\overline{u'v'}/(\overline{u'v'})_{0.3L}$

To reveal the normal distribution laws of the velocity fluctuation, Figure 10 gives the profiles of the resolved turbulent kinetic energy, $k_r$, at different streamwise locations. Where $k_r$ in there is calculated by the resolved Reynolds normal stress, which represents the total resolved velocity fluctuation in three direction. And $d_w$ is the distance from the location where $k_r$ have the maximum value ($k_{r\,max}$) to the nearest wall. The figure shows that the $d_w$ increases gradually with the development of the boundary layer. Meanwhile the magnitude of $k_{r\,max}$ grows rapidly in the downstream of $0.4L$. On the one hand this is caused by the development of fluctuation during transition. On the other hand, the appearance of adverse pressure gradient speeds up the transition process, which strengthen the magnitude of fluctuation. The $d_w$ and $k_{r\,max}$ for different streamwise locations are extracted from Figure 10 and plotted in Figure 11. Two curves (FC1 and FC2) are used to fit the discrete data of $k_{r\,max}$ and $d_w$ respectively, and the best fitting equations are as follows:

$$\text{FC1: } f(x/L) = 2.754\times10^{-5}e^{9.141x/L} \quad (6)$$

$$\text{FC2: } f(x/L) = 0.01831x/L + 0.3399 \quad (7)$$

It can be seen that the equation of FC1 is an exponential function, and the good fitting between FC1 and discrete data demonstrates that the $k_{r\,max}$ develops downstream approximately with an exponential growth during the transition process. In addition, the expression of equation (7) indicates that the ratio of

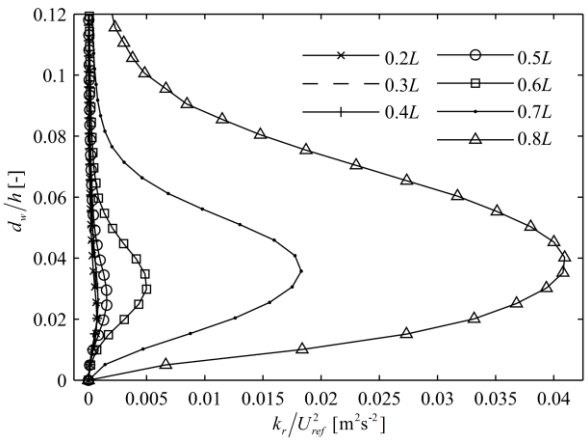


**Figure 10.** The profiles of the resolved turbulent kinetic energy, calculated by the Reynolds normal stress, at different streamwise locations

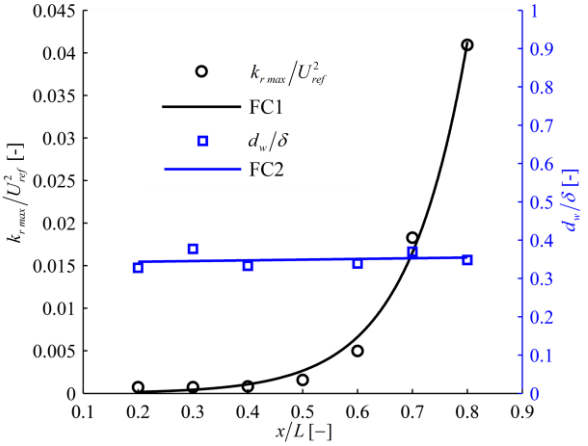


**Figure 11.** The profiles of the maximum resolved turbulent kinetic energy and its corresponding location in the local boundary layer along hydrofoil chord

$d_m$ to $\delta$ is almost constant considering the slope of FC2 is small enough. So it means that the fluctuation achieves the maximum value at the same relative location of the boundary layer for different streamwise locations.

## 4. Conclusion

Based on the WALE model, this paper presents a large eddy simulation of the boundary layer transition flow around the NACA0009 blunt trailing edge hydrofoil at high Reynolds number. The calculated results are analyzed and compared with the experimental data to obtain the transitional boundary layer structure and to validate the capability of WALE model in predicting the transition at high Reynolds number. In addition, the spatial velocity fluctuation profiles in the transitional boundary layer is analyzed to reveal the development laws. The main findings in this paper are as follows:

The WALE model-based large eddy simulation can accurately predict the hydrofoil boundary layer transition at high Reynolds number. After the transition, the boundary layer thickness and shape factor increase rapidly. Besides, the three dimensional eddies appear and develop downstream, and the interaction among eddies become stronger in this process.

There are obvious differences in the developments of the magnitude of velocity fluctuation for different layers of the boundary layer, but the profiles of fluctuation growth ratio are almost the same before the transition is completed.

The profiles of the fluctuation normal to the hydrofoil surface have the maximum value in almost the same relative location of the boundary layer for different streamwise locations, and the maximum value develops along hydrofoil chord approximately with an exponential increase.

## Acknowledgments

This work was funded by the National Natural Science Foundation of China (Grant Nos. 51679240).

## Reference

[1] Ingen J L V 1956 A suggested semi-empirical method for the calculation of boundary layer transition region *Technical Report of Delft University of Technology* Delft.
[2] Smith A M O and Gamberoni N 1956 Transition pressure gradient and stability theory *Technical Report of Douglas Aircraft Company* Long Beach California.
[3] Leylek J H and Walters D K 2004 A new model for boundary layer transition using a single-point

RANS approach *Journal of Turbomachinery* volume 126 issue 1 pp 193-202.
[4] Walters D K 2008 A three-equation eddy-viscosity model for Reynolds-averaged navier–stokes simulations of transitional flow *Journal of Fluids Engineering* volume 130 issue 12 pp 320-327.
[5] Menter F R, Langtry R B, Likki S R, et al 2006 A correlation-based transition model using local variables - part I: model formulation *Journal of Turbomachinery* volume 128 issue 3 pp 57-67.
[6] Ingen J V 2008 The eN method for transition prediction: historical review of work at TU Delft *AIAA 38th Fluid Dynamics Conference and Exhibit*.
[7] Smagorinsky J 1963 General Circulation Experiments with the Primitive Equations *Monthly Weather Review* volume 91 issue 3 pp 99-164.
[8] Nicoud F and Ducros F 1999 Subgrid-Scale Stress Modelling Based on the Square of the Velocity Gradient Tensor *Flow Turbulence & Combustion* volume 62 issue 3 pp 183-200.
[9] Weickert M, Teike G, Schmidt O, et al 2010 Investigation of the LES WALE turbulence model within the Lattice Boltzmann framework *Computers & Mathematics with Applications* volume 59 issue 7 pp 2200-2214.
[10] Kizildag D, Trias F X, Rodr ́guez I, et al 2014 Large eddy and direct numerical simulations of a turbulent water-filled differentially heated cavity of aspect ratio 5 *International Journal of Heat & Mass Transfer* volume 77 issue 77 pp 1084-1094.
[11] Boudet J, Monier J F and Gao F 2015 Implementation of a Roughness Element to Trip Transition in Large-eddy Simulation *Journal of Thermal Science* volume 24 issue 1 pp 30-36.
[12] Ausoni P 2009 Turbulent vortex shedding from a blunt trailing edge hydrofoil *PhD Thesis of École Polytechnique F éd érale de Lausanne* Lausanne.